








Classification of Aortic Stenosis Patients via ECG-Independent Multi-Site Measurements of Cardiac-Induced Accelerations and Angular Velocities at the Skin Level

Chiara Romano , Student Member, IEEE, Emanuele Maiorana , Senior Member, IEEE, Annunziata Nusca , Simone Circhetta, Sergio Silvestri , Schena Emiliano , Senior Member, IEEE, Gian Paolo Ussia , and Carlo Massaroni , Senior Member, IEEE

Abstract—Goal: To evaluate the suitability of seismocardiogram (SCG) and gyrocardiogram (GCG) recorded at the skin level to classify aortic stenosis (AS) patients from healthy volunteers, and to determine the optimal sensor position for the classification. **Methods:** SCG and GCG were recorded along three axes at five chest locations of fifteen healthy subjects and AS patients. Signal frames underwent feature extraction in frequency and time-frequency domains. Then, binary classification was performed through three machine learning and three deep learning methods, considering SCG, GCG, and their combination. **Results:** The highest classification accuracies were achieved using Support Vector Machine (SVM) classifier, with the best sensor locations being at the mitral valve for SCG signals (92.3% accuracy) and at the pulmonary valve for GCG (92.1%). Combining SCG and GCG data allows for further improvement in the achievable accuracy (93.5%). Jointly exploiting SCG and GCG signals and both SVM- and ResNet18-based classifiers, 40 s of monitoring allows for reaching 97.2% accuracy with a single sensor on the pulmonary valve. **Conclusions:** Combining SCG and GCG with

adequate machine learning and deep learning classifiers allows reliable classification of AS patients.

Index Terms—Wearables, seismocardiogram, gyrocardiogram, machine learning, aortic stenosis (AS), sensors.

Impact Statement— Cardiac-induced accelerations and angular velocities at the skin level allow classifying aortic stenosis patients.

I. INTRODUCTION

AORTIC stenosis (AS) is among the three most common valvular heart diseases in Western countries, occurring in about 3% of patients over 75 years of age [1]. Major risk factors for the development of AS include hypertension and metabolic diseases. Hence, recent observational studies reported that due to the increasing prevalence of these cardiac risk factors, around 2% of people aged 55 years or older are already living with severe AS in high-income countries [2], [3]. This cardiovascular disorder is caused by a degenerative calcification of the valvular cusps, which increases leaflet stiffness and reduces the systolic valvular opening, increasing the mean pressure gradient (ΔP) between the left ventricle (LV) and the aorta [4], [5]. The typical course of AS includes a prolonged asymptomatic period, after which severe symptoms might appear once a significant reduction in stroke volume occurs over time [4], [5]. According to guidelines, severe AS is defined by a ΔP between the LV and aorta above 40 mmHg, an aortic valve area (AVA) smaller than 1 cm², and a peak aortic jet velocity across the valve higher than 4.0 m/s [6], [7], [8]. These parameters are commonly obtained by performing an echocardiogram (hereinafter echo) [9], [10]. However, these current echo parameters could lose their reliability in some specific AS settings, provoking an under-detection and underestimation of the severity of this valvular defect. Indeed, inconsistencies in the echo metrics may occur in the presence of left ventricular dysfunction where peak aortic jet velocity and ΔP might be less than 4 m/s and 40 mmHg, respectively, also in the presence of severe AS [11]. If the disease is not detected, it will, of course, not be treated or treated too late. Unfortunately, late diagnosis and late referral for treatment

Manuscript received 3 January 2024; revised 28 March 2024, 7 May 2024, and 14 May 2024; accepted 14 May 2024. Date of publication 20 May 2024; date of current version 7 November 2024. This work was supported in part by the European Project PROVIDE ("Prediction and prevention of cardiovascular diseases in pre- and type 2 diabetes", call topic EU4H-2022-PJ-1) under Grant 101128983. The review of this article was arranged by Editor Riccardo Barbieri. (Chiara Romano and Emanuele Maiorana contributed equally to this work.) (Corresponding author: Carlo Massaroni.)

Chiara Romano and Sergio Silvestri are with the Research Unit of Measurements and Biomedical Instrumentation, Department of Engineering, Università Campus Bio-Medico di Roma, 00128 Rome, Italy.

Emanuele Maiorana is with the Biometric Systems and Multimedia Forensics (BioMedia4n6) Laboratory of the Department of Industrial, Electronic and Mechanical Engineering, Roma Tre University, 00146 Rome, Italy.

Annunziata Nusca, Simone Circhetta, and Gian Paolo Ussia are with the Fondazione Policlinico Universitario Campus Bio-Medico, 00128 Rome, Italy, and also with the Research Unit of Cardiac Sciences, Department of Medicine and Surgery, Università Campus Bio-Medico di Roma, 00128 Rome, Italy.

Schena Emiliano and Carlo Massaroni are with the Research Unit of Measurements and Biomedical instrumentation, Department of Engineering, Università Campus Bio-Medico di Roma, 00128 Rome, Italy, and also with the Fondazione Policlinico Universitario Campus Bio-Medico, 00128 Rome, Italy (e-mail: c.massaroni@unicampus.it).

Digital Object Identifier 10.1109/OJEMB.2024.3402151

are common in the AS field, with tremendous consequences on the outcomes and survival of these patients [12].

Additional advanced imaging tests such as computed tomography (CT) or cardiac magnetic resonance imaging (MRI) could be performed to obtain more detailed images of the heart and its valves [9], [10]. During CT, images of the heart are acquired using X-rays from various angles. Subsequently, these images are reconstructed into three-dimensional images. CT can be used to assess the size and shape of the aortic valve and to identify the presence of cusp calcifications. However, CT is not ideal for evaluating the function of the aortic valve and the amount of blood flow passing through the valve. MRI uses magnetic fields and radio waves. During the scan, a series of images of the heart from different angles are acquired, which are then reconstructed into three-dimensional images [13].

Unlike CT, MRI can be used to assess the function of the heart valve and the amount of blood flow passing through it. However, MRI may be less accurate than CT in evaluating the presence of aortic calcifications [13].

These techniques have limitations primarily related to their invasiveness, complexity, and costs. In fact, advanced imaging techniques such as echocardiography, CT, and MRI require the use of expensive equipment and the presence of highly specialized personnel during diagnostic examinations [14].

For all these reasons, new solutions that involve the use of wearable sensors are emerging. These devices show great promise in various fields, including the clinical-diagnostic realm, particularly in the cardiac domain. The introduction of wearable sensors in the cardiac field represents a new frontier in the diagnosis and monitoring of cardiovascular diseases, including AS. 12-lead and single-lead ECG, in conjunction with deep learning (DL) algorithms, have been demonstrated to be potentially reliable screening tools for detecting significant AS [15]. However, biopotential recording suffers limitations as the ECG signal quality may be affected by noise and other confounding factors, especially when wearable devices are used, caused by skin-impedance changes, motion artifacts, and improper device installation. As an alternative to ECG recording, a promising solution is represented by sensors enabling recording vibrations induced by the heart in the form of linear accelerations (called seismocardiogram, hereinafter SCG) and angular velocities (called gyrocardiogram, hereinafter GCG) of the chest's surface to which they are attached. The operating principle is further detailed in Section II-A. The SCG and GCG have found application in the diagnosis of various cardiovascular diseases, such as aortic valve diseases [16], myocardial infarction [17], [18], atrial fibrillation [19], [20], and heart failure [17], [21], and in monitoring the effects of cardiac resynchronization therapy [22]. However, only a few studies in the literature tried to classify AS based on cardio-mechanical recordings, and they always used ECG to delineate SCG and GCG templates [23], [24], [25]. This strongly limits our knowledge about the applicability of SCG and GCG in recognizing AS patients without the support of a synchronized ECG signal.

Moreover, it is necessary to observe other limitations of the current state of the art in the field. All previous investigations that have attempted to classify AS suggested measuring SCG and sometimes GCG through magneto-inertial sensors placed on straps or bands around the thoracic cage, typically at the centre of the sternum [23], [24], [25], [26], [27]. This position, anatomically difficult to reproduce across studies, is prone to sensor placement errors and does not guarantee the absence of sensor displacement during measurement. To date, no study has employed wearable sensors in close contact with the skin surface, potentially improving the quality of the collected data. Additionally, none of the studies have yet explored multiple positions on the ribcage to optimally record SCG and GCG signals relevant to classifying patients with AS. In a previous study conducted by our research group, for instance, we demonstrated that cardiac monitoring of heart rate (HR) using magneto-inertial sensors is more accurate when the sensor is intimately placed in contact with the chest around the mitral valve area, even though literature typically positions magneto-inertial sensors nearby the xiphoid process [28].

To tackle all these limitations, our study focuses on the multi-site (five sensors) and multi-dimensional (three-axis) registration of accelerations and angular velocities induced by cardiac vibrations using magneto-inertial units with sensors intimately attached to the skin. We carried out experiments on both healthy volunteers and patients with severe AS. The multidimensional and distributed signals from SCG and GCG are employed to classify AS patients, utilizing various ECG-independent Machine Learning (ML) and DL algorithms. The objectives of this research are threefold: 1) to assess the performance of classifiers in accurately distinguishing AS patients from healthy volunteers, exclusively based on SCG and GCG signals, 2) to explore the advantages resulting from the fusion of information extracted from both SCG and GCG signals, and 3) to determine the optimal sensor position, guiding further research in this domain.

II. MATERIALS AND METHODS

A. SCG and GCG Signals

Each cardiac cycle involves the heart twisting forward and touching the chest wall. As a result, vibrations in the chest can be detected with an accelerometer or a gyroscope attached to the sternum. The accelerometer records the linear acceleration of the chest (SCG), while the gyroscope records the angular velocity of the chest (GCG). Typically, the SCG signal is recorded using the dorsoventral axis of the accelerometer positioned on the xiphoid process. Since the 1990 s, SCG has been used to measure the motion of the myocardium during ventricular contraction [29], [30]. Later, studies suggested that some fiducial points on the dorsoventral SCG signal were associated with aortic and mitral valve opening and closing events, as shown in Fig. 1 [31]. More recently, a gyroscope placed on the sternum was used to collect GCG signals. This consists of recording the angular velocity of the chest caused by the heart's rotation. The rate of the angular

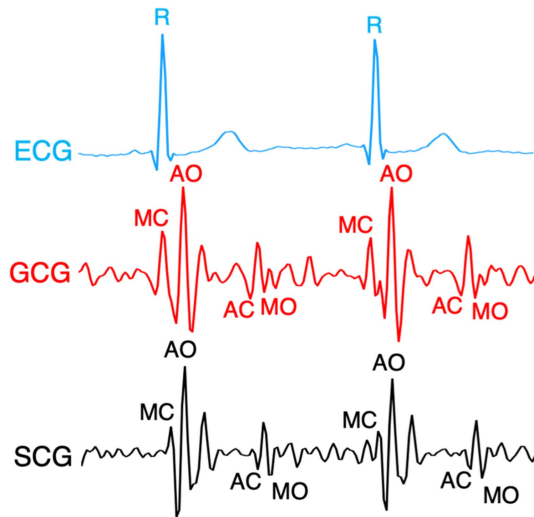


Fig. 1. Simultaneous recordings of ECG, GCG (shoulder-to-shoulder direction), and SCG (dorsoventral direction). MC and MO: mitral valve closure and opening; AC and AO: aortic valve closure and opening.

velocity of the thorax can be described as the speed of rotation and the axis around which it rotates. As for the SCG, the GCG has also been defined as a new technique for monitoring the heart timing intervals exhibiting fiducial points related to the opening and closure of the aortic valve and mitral valve [32], [33], [34]. An example in which SCG and GCG signals are compared to an ECG signal is shown in Fig. 1.

B. Experimental Set-Up and Protocol

This study includes fifteen healthy subjects -healthy group- (4 males and 11 females, age: 26 ± 3 years, body mass: 61 ± 10 kg, BMI: 21 ± 2 kg/m², expressed as mean \pm standard deviation) without evidence of cardiovascular diseases and fifteen AS patients (8 male and 7 females, age: 80 ± 12 years, body mass: 72 ± 14 kg, BMI: 26 ± 5 kg/m²). Among AS patients, fourteen were diagnosed with severe AS, while one was diagnosed with moderate AS. The AS severity was assessed through an ultrasound examination performed by specialized physicians combined with the measurement of the main hemodynamic parameters during left heart catheterization, as summarized in Table I. These values were used to evaluate the severity of AS and classified it as either mild ($AVA > 1.5$ cm², $AVA/BSA \geq 1.0$ cm²/m², 2.6 m/s $\leq V_{max} \leq 2.9$ m/s, $\Delta P \leq 20$), moderate (1.0 cm² $\leq AVA \leq 1.5$ cm², 0.6 cm²/m² $\leq AVA/BSA \leq 0.85$ cm²/m², 3.0 m/s $\leq V_{max} \leq 4.0$ m/s, $20 \leq \Delta P \leq 40$), or severe ($AVA < 1.0$ cm², $AVA/BSA < 0.6$ cm²/m², $V_{max} > 4.0$ m/s, $\Delta P > 40$) [35].

Linear accelerations and angular velocities of the rib cage were recorded using commercial inertial measurement unit (IMU) sensors (Xsens Technologies B.V., Enschede, Netherlands) located at five different points of the thorax, as shown in Fig. 2.

The placement of the sensors before the test was guided by an expert physician, who placed them at the levels of the main areas

TABLE I
MAIN HEMODYNAMIC PARAMETERS OF AS PATIENTS

Patient number	AVA [cm ²]	AVA/BSA [cm ² /m ²]	V_{max} [m/s]	ΔP [mmHg]
1	0.8	0.47	4.01	45
2	0.6	0.28	4.78	50
3	NE	NE	5.04	NE
4	1.0	0.62	3.23	NE
5	0.5	0.29	3.58	36
6	0.7	0.41	3.07	25
7	0.8	0.41	3.51	NE
8	0.4	0.24	NE	15
9	0.8	0.39	5.40	NE
10	NE	NE	4.20	NE
11	0.7	0.39	3.98	40
12	0.4	0.26	4.60	75
13	0.9	0.58	2.67	NE
14	0.8	0.45	NE	12
15	0.45	0.30	3.88	30

NE: Not Executed; AVA: Aortic Valve Area; BSA: Body Surface Area; ΔP : pressure gradient between aorta and left ventricle; V_{max} : peak velocity.

of heart auscultation in a patient in a supine position. Specifically, they were positioned to correspond with the aortic valve (AO), mitral valve (MV), tricuspid valve (TV), pulmonary valve (PV), and with the xiphoid process (X) by using bi-adhesive medical tape typically employed in motion capture recordings [36]. The main 5 areas were identified through the palpation of the precordium, as usually performed during cardiac examination, and confirmed the sensors position by using fluoroscopy during left/right catheterization and coronary angiography. Each IMU sensor embeds a triaxial accelerometer and a triaxial gyroscope to record SCG and GCG, respectively.

Hence, both the SCG and GCG signals were recorded along the x-axis (defined as the head-to-toe direction), y-axis (defined as the shoulder-to-shoulder direction), and z-axis (defined as the anterior-posterior direction).

Regarding the healthy group, data were collected at the University Campus Bio-Medico di Roma. The recruitment was accomplished in adherence to the Declaration of Helsinki and after the ethics committee approval of our institution (Prot. PAR 04.22 OSS). As described above, the five IMU sensors were placed on the thorax at the skin level. Subsequently, each subject was instructed to assume a lying position and the SCG and GCG signals were collected for 120 s at a sampling rate of 120 Hz.

Data from the AS group were recorded during the cardiac catheterization preceding the transcatheter aortic valve implantation (pre-TAVI), at the Cardiology Unit of the Fondazione Policlinico Universitario Campus Bio-Medico, Rome, Italy. During this procedure, a catheter is inserted into the heart chambers under fluoroscopy guidance to measure intracardiac pressures and hemodynamic parameters, with insertion occurring intermittently during specific phases of the cardiac catheterization procedure rather than continuously throughout.

The recruitment was accomplished in adherence to the Declaration of Helsinki and after the ethics committee approval of our institution (Prot. PAR 04.22 OSS). All participants provided written informed consent to participate in the study. Before the

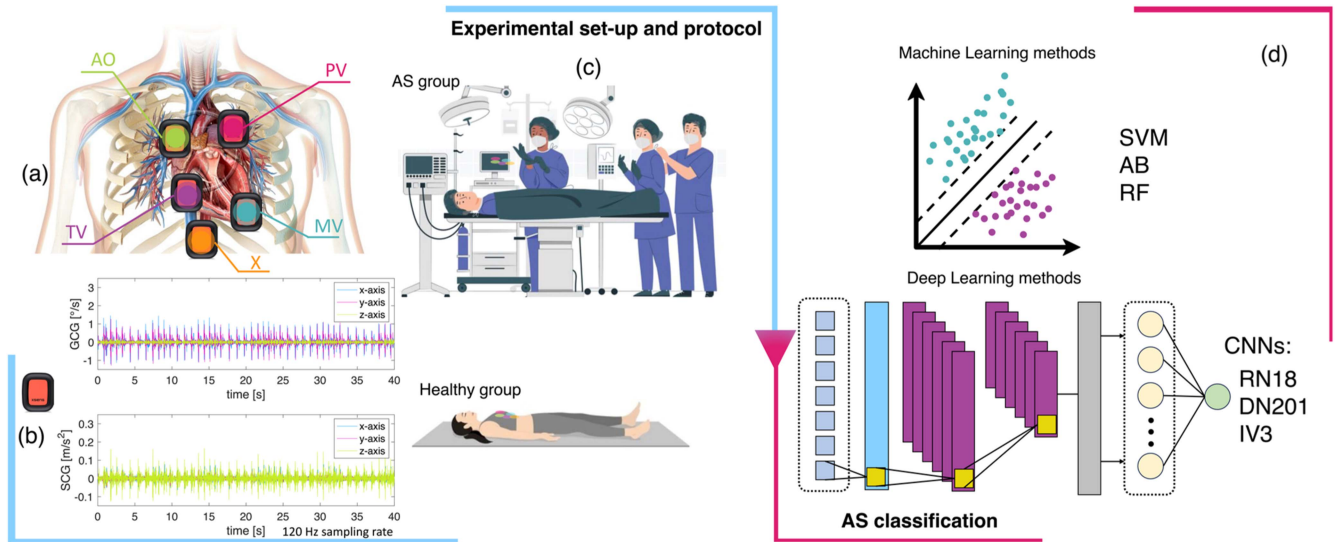


Fig. 2. (a) Schematic representation of the positioning of the five IMU sensors on the chest (in the positions AO: aortic valve, PV: pulmonary valve, TV: tricuspid valve, X: xiphoid process, MV: mitral valve); (b) Example of SCG (along x, y and z axes) and GCG (along x, y, z axes) signals collected during a test with a lying subject; (c) Schematic representation of the protocol for the healthy group and the AS group; (d) Algorithms used for AS classification.

procedure, the five IMU sensors were placed on the thorax of the AS patients when lying on the operating table. Subsequently, the SCG and GCG signals were recorded while measuring intracardiac pressures for the entire duration of the procedure (about 1h) at a sampling rate of 120 Hz. Subsequently, 120 s segments were selected from the one-hour recording after visual inspection, ensuring that the chosen segments displayed minimal motion artifacts and clearly visible cardiac peaks.

SCG and GCG signals of both the healthy and AS groups were stored in the internal memory of the IMU sensors and then downloaded to the computer for further analysis. In addition, hemodynamic parameters obtained following the physician's evaluation of cardiac catheterization were considered per each subject, as reported in Table I.

C. Signal Pre-Processing

The collected signals were pre-processed in MATLAB 2023a environment. First, a finite impulse response (FIR) band-pass filter with cut-off frequencies of 0.1 Hz and 30 Hz was applied to all axes of SCG and GCG signals. This allowed us to select only the signal frequencies related to the cardiac mechanical activity. Then, each signal was resampled at $R = 60$ Hz to reduce the computational complexity of the subsequent processing.

The resulting signals were then segmented into overlapping frames, using rectangular time windows of length $L = 10$ s with an overlap $O = 80\%$, allowing a separation of 2 s between consecutive segments. A set with $K = \lfloor 1 + \frac{1}{1-O} (\frac{S}{L} - 1) \rfloor = 56$ frames, each comprising $A = 3 \cdot (L \cdot R)$ samples considering all three axes, is thus generated from each original SCG or GCG acquisition lasting $S = 120$ s. The frames thus created were treated as individual samples in the considered systems, meaning that an inference about the presence of AS conditions is carried out on the basis of a single frame lasting L seconds,

while the training of the employed classifier was conducted relying on the availability of a set of segments each lasting $L = 10$ s.

D. Signal Representations

The pre-processed signals were further treated in order to generate the representations fed to the employed classifiers. Specifically, the frequency and time-frequency domains were exploited to this aim, considering respectively the power spectral density (PSD) and the absolute values of the short-time Fourier Transform (STFT) of the considered frames. Using a frequency resolution of $1/3$ Hz, subframes lasting 3 s with an overlap of 98%, and Chebyshev windows for subframe division when computing STFT, the obtained representations contain 3 (channels) $\cdot 30$ (Hz) $\cdot \frac{1}{1/3}$ (resolution) = 90 features for the PSD, and $3 \cdot 90 \cdot 106 = 28620$ features (due to the used MATLAB implementation), arranged as $[90 \times 106]$ planes of a 3D tensor, for the STFT representations.

It is worth mentioning that the performed division into frames was carried out without any reference to the occurrence of specific cardiac events, such as valve closure or opening, in the processed signals. While the PSD representation contains only frequency-related content, making it fairly independent from the temporal behavior, the representations in the STFT domain depend on the performed frame temporal division. In order to properly handle these latter, translation-invariant classifiers should be therefore employed.

E. Classifiers

An extensive set of binary classifiers was considered to evaluate the feasibility of estimating whether or not a subject exhibit AS on the basis of non-invasive measurements from IMU

sensors. Specifically, both classic ML approaches as well as DL frameworks were considered in the performed study.

As for classic ML algorithm [37], approaches based on support vector machines (SVMs) and ensembles of classification trees were exploited. In more detail, SVMs with a Gaussian kernel were considered, while both random forest (RF) and AdaBoost (AB) were employed as tree ensembles. All the considered classic ML classifiers were fed with PSD representations of SCG and GCG frames. The possibility to jointly exploit SCG and GCG signals with classic ML methods was also investigated, by using concatenations of the PSD features from accelerometer and gyroscope as input of the classifiers.

As for DL approaches, convolutional neural networks (CNNs) were exploited to derive discriminative information from the computed STFT representations. In more detail, since the employed IMU sensors provide data along three axes, the 3D tensors with the STFT representation of either SCG or GCG signals were used as inputs of networks originally proposed to perform image classification, after being resized to comply with the requirements of the used architectures. It is worth noting that STFT representations can be properly used jointly with CNNs even if the segmentation of the original signals into frames of L seconds is performed without reference to specific events, thanks to the translation-invariant capability that characterizes neural networks relying on convolutions.

Transfer learning is exploited to adapt networks pre-trained on ImageNet [38] for the task here considered, fine-tuning them on SCG or GCG training data for a binary task, using a cross-entropy loss function for back-propagation, stochastic gradient descent (SGD) with momentum set at 0.9, and a batch size of 16. To perform a thoughtful evaluation of this approach, several effective networks proposed in literature were considered in the performed tests, namely ResNet18 (RN18) [39], InceptionV3 (IV3) [40], and DenseNet201 (DN201) [41]. To adapt the aforementioned networks for the considered task, their last layer was modified to handle binary classification tasks, and all their preceding layers were fine-tuned using the available training data. Those specific networks were selected to test solutions with different computational complexities, with DN201 typically demanding more training and predictive time than IV3, which, in turn, has higher computational requirements than RN18.

Pre-trained networks were also employed to design a strategy relying on deep learning to jointly exploit both SCG and GCG data. In more detail, to achieve this goal, it is not possible to combine both sources of information at a feature level as done with standard classifiers since it is not possible to use tensors with six planes (three for SCG and three for GCG) as input to the employed pre-trained networks. Moreover, accelerometer and gyroscope data cannot be combined along the other two dimensions since such an approach would not result in a proper use of CNN properties. A score-fusion strategy was therefore adopted by first fine-tuning pre-trained networks on SCG and GCG information separately. When a decision has to be taken for a probe frame, accelerometer and gyroscope data extracted from the same time window are fed to the networks

fine-tuned on the two kinds of signals, and the two produced outcomes, i.e., the two expected probabilities of AS conditions, are averaged to produce a single score, used to take a decision on the basis of predictions performed on both SCG and GCG data.

III. RESULTS

The collected database, with acquisitions taken from 15 AS patients and 15 healthy subjects, was used to evaluate the capability of estimating AS by means of a user-convenient setup based on wearable inertial sensors.

The first objective of the performed test was to assess the effectiveness of using SCG or GCG signals for the proposed task and evaluate the improvements achievable by resorting to both of the considered kinds of data. To this aim, a 5-fold cross-validation evaluation strategy was used in the performed test by selecting from the available dataset, for five different iterations, 80% of the AS and healthy subjects to provide data for training and validation (10% of considered data used for validation), and the remaining ones for the testing samples. This way, disjoint sets of subjects were always considered for training and testing purposes, thus guaranteeing the generalizability of the obtained results. In more detail, each iteration was carried out $56 \cdot (30 \cdot 0.8) = 1344$ frames from 24 subjects for training and validation purposes, and $56 \cdot (30 \cdot 0.2) = 336$ frames from 6 subjects for performance evaluation.

Table II reports the accuracies obtained when employing SCG and GCG from sensors placed in different positions and exploiting different classifiers. From the obtained results, it can be seen that, in general, the best performance can be obtained when considering SCG signals recorded at the MV position and GCG data collected at the PV position. For the other sensor locations, considering GCG data typically allows us to achieve better results than using SCG signals. It is, therefore, evident that selecting the place where to locate the employed inertial sensors has significant effects on the reliability of the performed predictions.

The reported accuracies also show that combining SCG and GCG data allows for further improvement in the achievable performance. In more detail, jointly exploiting accelerometer and gyroscope information allows for reducing the performance variability among different positions, with PV and MV locations still preferable over the others. However, the results obtained are significantly more uniform between the distinct sensor placements.

A statistical analysis was also performed to draw more significant information from the results obtained. In more detail, ANOVA tests were conducted on the results obtained considering SCG and GCG collected at different position, to evaluate whether the achieved performance shows significant differences among different classifiers. Considering SCG signals, a p-value at 2.18% was obtained for the MV position, with subsequent Tukey's honest significant difference (HSD) tests revealing relevant differences at 5% significance level when comparing SVM against AB, IV3, and DN201. For GCG signals, a p-value at 1.15% was obtained for ANOVA tests on the PV position,

TABLE II

RECOGNITION PERFORMANCE, IN TERMS OF ACCURACY (MEAN \pm STANDARD DEVIATION, IN %), FOR A SINGLE FRAME LASTING 10s USED AS PROBE, CONSIDERING SCG AND GCG SENSORS PLACED AT DIFFERENT POSITIONS, AND DIFFERENT CLASSIFIERS.

Signal	Position	Classifier					
		SVM	RF	AB	RN18	IV3	DN201
SCG	PV	80.8\pm5.6%	77.7 \pm 6.0%	77.3 \pm 6.8%	78.1 \pm 6.2%	75.7 \pm 7.7%	77.5 \pm 6.8%
	AO	77.7\pm7.1%	67.4 \pm 6.0%	69.4 \pm 6.9%	72.9 \pm 5.6%	68.7 \pm 6.8%	69.1 \pm 7.8%
	X	74.5\pm6.9%	67.1 \pm 5.9%	62.7 \pm 8.5%	69.1 \pm 6.6%	67.3 \pm 7.1%	62.7 \pm 7.6%
	MV	92.3\pm3.9%	86.2 \pm 2.7%	84.6 \pm 3.3%	86.5 \pm 3.9%	84.1 \pm 3.6%	85.8 \pm 4.3%
	TV	75.5 \pm 6.6%	72.9 \pm 6.3%	75.9 \pm 6.2%	77.4\pm6.1%	73.7 \pm 7.4%	73.4 \pm 6.7%
GCG	PV	92.1\pm3.4%	82.1 \pm 3.8%	82.4 \pm 5.5%	84.1 \pm 4.6%	83.2 \pm 3.9%	84.5 \pm 4.2%
	AO	83.4\pm6.8%	79.1 \pm 5.2%	78.5 \pm 5.8%	79.6 \pm 4.7%	78.9 \pm 4.0%	78.1 \pm 5.2%
	X	84.7\pm5.4%	78.4 \pm 7.3%	75.4 \pm 8.0%	79.2 \pm 3.3%	78.9 \pm 3.8%	81.9 \pm 3.6%
	MV	74.9 \pm 4.5%	72.4 \pm 2.6%	76.2 \pm 3.5%	78.3\pm6.3%	78.1 \pm 7.7%	75.5 \pm 8.7%
	TV	83.9 \pm 3.4%	79.5 \pm 6.2%	79.0 \pm 4.8%	85.1\pm4.9%	84.8 \pm 5.3%	83.8 \pm 5.6%
SCG+ GCG	PV	92.8\pm3.2%	83.1 \pm 3.4%	85.5 \pm 4.7%	85.7 \pm 5.1%	89.8 \pm 4.1%	86.9 \pm 4.4%
	AO	84.6\pm5.6%	79.8 \pm 5.4%	78.7 \pm 5.7%	82.3 \pm 4.8%	82.8 \pm 4.5%	81.2 \pm 5.4%
	X	85.0\pm4.9%	80.2 \pm 5.8%	78.4 \pm 7.2%	79.6 \pm 3.8%	81.4 \pm 4.1%	79.9 \pm 4.2%
	MV	93.5\pm2.6%	86.8 \pm 1.9%	87.1 \pm 2.8%	87.6 \pm 4.5%	85.5 \pm 4.2%	86.7 \pm 4.8%
	TV	84.1 \pm 3.6%	81.9 \pm 4.9%	84.6 \pm 4.4%	86.1 \pm 4.1%	87.6\pm5.9%	86.4 \pm 5.8%

SVM: Support Vector Machine, RF: Random Forest, AB: AdaBoost, RN18: ResNet18, IV3: InceptionV3, DN201: DenseNet201
 AO: Aortic valve, MV: Mitral valve, TV: Tricuspid valve (TV), pulmonary valve (PV), and with the xiphoid process (X)
 The best Results for each type of input and sensor position are reported in bold.

with HSD tests revealing relevant differences when comparing SVM against all the other classifiers. When jointly exploiting SCG and GCG data, p-values at 1.84% and 2.79% were respectively obtained for ANOVA tests on the PV and MV positions, with significant differences between SVM and RF for PV, and between SVM and all the other classifiers apart from RN18 for MV. Tests performed using CNNs therefore do not show improvements when selecting networks with a computational complexity higher than RN18. This behavior may be since the amount of data available for training purposes is relatively limited and probably not enough to perform an effective fine-tuning of complex frameworks.

Further ANOVA tests were conducted to evaluate whether there are significant differences among the results obtained when placing sensors at different positions. For SCG, the ANOVA test performed provided a p-value at 0.14%, with subsequent HSD tests revealing significant differences between MV and all the other locations. For GCG, a p-value at 1.45% was obtained in the ANOVA test, for differences between PV and MV locations. The use of both SCG and GCG resulted in a p-value at 1.28% for differences of PV and MV against AO.

In order to evaluate whether further enhancements could be attained, tests were performed to evaluate the effectiveness of jointly exploiting two classifiers. With no claim for optimality, we selected SVM and RN18 for this analysis, and evaluated the performance achievable when summing the prediction scores independently produced by both of them, after having performed a normalization to the same range, before taking a decision. Table III reports the performance in terms of accuracy, precision,

TABLE III

RECOGNITION PERFORMANCE, IN TERMS OF ACCURACY (MEAN \pm STANDARD DEVIATION, IN %), FOR A SINGLE FRAME LASTING 10s USED AS PROBE, CONSIDERING SENSORS PLACED AT DIFFERENT POSITIONS, JOINTLY EXPLOITING SCG AND GCG SIGNALS, AND BOTH SVM- AND RN18-BASED CLASSIFIERS

Position	Accuracy	Precision	Recall	F1-score
PV	93.9 \pm 3.2%	95.37 \pm 2.0%	92.1 \pm 4.8%	93.5 \pm 3.5%
AO	85.2 \pm 5.1%	86.35 \pm 6.1%	87.1 \pm 5.6%	85.6 \pm 4.5%
X	87.2 \pm 5.7%	86.03 \pm 5.9%	89.5 \pm 4.9%	87.7 \pm 5.4%
MV	93.7 \pm 2.7%	96.18 \pm 2.1%	90.9 \pm 4.4%	93.3 \pm 2.9%
TV	87.5 \pm 3.8%	87.24 \pm 5.1%	89.2 \pm 3.3%	87.8 \pm 4.0%

recall, and F1-score obtained for sensors placed in different positions, jointly using SCG and GCG data and combining the outcomes of SVM and RN18 classifiers. Significant differences were still found when comparing PV and MV positions against AO, for a p-value at 0.96% in an ANOVA test on accuracies.

It is worth mentioning that the results so far reported are referred to predictions carried out based on SCG and GCG frames lasting 10 s. Nonetheless, when longer acquisitions are available, it would be possible to exploit multiple frames to estimate the patients' conditions, by leveraging on a score-level information fusion approach, that its, performing a decision over the available probe based on the average prediction scores computed for each processed frame. Following such approach, the behavior

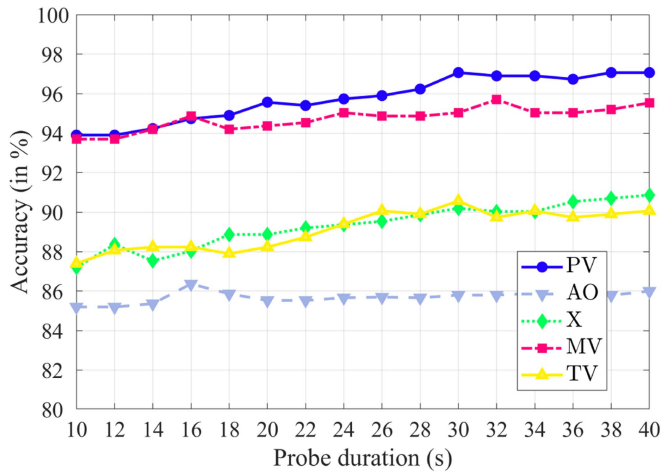


Fig. 3. Mean recognition accuracies obtained in the performed cross-validation tests for increasing probe durations, obtained jointly exploiting SCG and GCG signals, used as inputs to SVM- and RN18-based classifiers. The outcomes obtained from analyzing different frames are fused at a score level.

reported in Fig. 3 can be achieved. As can be seen, accuracies above 95% can be attained by considering acquisitions taken at PV or MV positions and lasting 40 s.

For the same durations, data collected at X or TV positions allow us to achieve accuracies greater than 90%, while signals associated with the AO position provide the worst results in the performed tests.

IV. DISCUSSIONS

In this work, heart-induced linear acceleration and angular velocities data were acquired in healthy volunteers and AS patients with five IMU sensors directly attached to the skin at the AO, MV, TV, PV, and X levels. The objective was to evaluate the suitability of SCG and GCG in distinguishing healthy volunteers from AS patients. Also, the measurements of SCG and GCG in the five body sites allowed us to further investigate optimal sensor position to record data for classification purposes.

For the binary classification, both classic ML and DL classifiers have been implemented and tested. Specifically, SVM, RF, and AB were employed as classic ML algorithms, while RN18, IV3, and DN201 were used as DL approaches. A 5-fold cross-validation method was employed, involving five separate iterations where 80% of AS patients and healthy subjects from the available dataset were chosen for training purposes, with the rest used for testing. This approach ensured that different sets of subjects were used for training and testing in each iteration, thereby enhancing the reliability and generalizability of the obtained results.

As reported in Table II, the best classification accuracy among the evaluated classifiers is obtained with SVM and RN18. Also, the tests carried out with the other CNNs indicate that choosing networks with greater computational complexity does not lead to improved results. Considering the SCG, the best classification is obtained when the data are collected at MV level with an accuracy of $92.3 \pm 3.9\%$. Differently, GCG exhibits

TABLE IV

AGE REGRESSION PERFORMANCE, IN TERMS OF RMSE, FOR A SINGLE FRAME LASTING 10s USED AS PROBE (RMSE = 27.8 USING MEAN AGE AS PREDICTED VALUE)

Pos.	Least-squares			SVM		
	SCG	GCG	SCG+GCG	SCG	GCG	SCG+GCG
PV	24.6	27.3	22.4	22.8	26.6	21.3
AO	26.8	21.9	22.3	26.1	20.8	20.7
X	27.5	20.5	20.9	26.5	20.5	20.5
MV	20.7	27.3	20.3	20.5	27.7	20.3
TV	25.3	24.1	26.1	25.4	23.2	24.1

better accuracy ($92.1 \pm 3.4\%$) when recorded at the level of PV. Both these results are obtained considering SVM classifier. The performance improves by combining SCG and GCG data, with PV and MV locations still preferable over the others and an accuracy of $92.8 \pm 3.2\%$ and $93.5 \pm 2.6\%$, respectively. In both cases, the AO position does not demonstrate optimal performance, even though it might be expected to be the ideal body landmark for identifying alterations of angular velocities and linear accelerations between healthy individuals and AS patients. However, this can be explained by the fact that in hearts with AS, the developing hypertrophy of the left ventricle causes a slight rotation of the heart towards the right, meaning that the left ventricle becomes more anterior and central compared to normal. The obtained accuracy values are slightly lower compared to those of [42], which reached an accuracy of 98% with a sensor on the chest, but using a CNN with a leave-subject-out cross-validation. However, are in line with those of [23] where the classification is based on SCG and GCG morphological characteristics and heart rate variability parameters. This result offers new insights compared to previous studies where sensors were positioned near the center of the sternum.

Focusing on the joint use of SCG and GCG signals, classification results improve for all the sensor positions, in accordance with [27]. Our results show that even in this case, SVM was the most powerful classifier. As reported in Table IV, no other study has identified SVM and RN18 as the best classifiers, although it should be clarified that often this classifier was not even analyzed due to the complexity of the datasets and the features used for classification.

Lastly, by merging results obtained in position analysis and classifiers, Fig. 3 shows the classification accuracies obtained jointly using SCG and GCG data and combining the outcomes of SVM and RN18 classifiers. With only 40 s of data recorded by the user, accuracies above 95% can be attained by considering acquisitions taken at PV or MV positions, with greater values from PV (97.2%).

It is worth mentioning that a concern regarding the reliability of the performed study may derive from the notable differences in age between the AS and control groups. To evaluate whether such variations could produce potential bias in the AS decision-making process, we performed tests to assess the feasibility of predicting a subject's age leveraging on the availability of SCG and GCG measurements. As for the considered classic ML classifiers, we used the PSD representations of SCG and GCG frames as age predictors and employed both support vector

TABLE V
COMPARISON WITH PREVIOUS WORK

<i>Ref.</i>	<i>Signal</i>	<i>Sensor Position</i>	<i>Classifier</i>	<i># of Subjects</i>	<i>Instances</i>	<i>Accuracy [%]</i>
[23]	SCG+GCG+ECG*	Center of the sternum	XGBoost	45 (13 healthy, 32 AS)	training: 1868 test: 468	96.4
[24]	SCG+GCG+ECG*	Center of the sternum	RF	40 (20 healthy, 20 AS)	total: 480, 10-fold cross validation	99.4
[25]	SCG+GCG+ECG*+PPG*	Center of the sternum	RF	40 (20 healthy, 20 AS)	training: 960 test: 176, 10-fold cross validation	98.9
[25]	SCG+ECG*+PPG*	Center of the sternum	RF	40 (20 healthy, 20 AS)	total: 540, 10-fold cross validation	95.9
[27]	SCG+GCG	ND	XGBoost	33 (13 healthy, 21 AS)	total: 910, leave-subject-out	93.0
[26]	SCG+ECG*	Center of the sternum	RF	36 (20 healthy, 16 AS)	training: 11398 test: 1266, 10-fold cross validation	99.4
[42]	SCG+GCG+ECG*	ND	CNN	71 (51 healthy, 20 AS)	total: 34476, leave-subject-out	98.4
Our work	Jointly SCG+GCG	PV, AO, X, MV, TV	Jointly SVM+RN18 (10 s)	30 (15 healthy, 15 AS)	training: 1344 test: 336, 5-fold cross validation	PV: 93.9 AO: 85.2 X: 87.2 MV: 93.7 TV: 87.5
	Jointly SCG+GCG	PV	Jointly SVM+RN18 (40 s)	30 (15 healthy, 15 AS)	training: 1344 test: 336, 5-fold cross validation	97.2

ND: Not Declared; RF: random forest; XGBoost: extreme gradient boosting; CNN: convolutional neural network; SVM: support vector machine; AV: aortic valve; MV: mitral valve; TV: tricuspid valve; PV: pulmonary valve; X: xiphoid process; *: used for signal segmentation; CVDs: cardiovascular diseases; ECG: electrocardiogram; PPG: photoplethysmogram.

machine (SVM) and least-squares (LS) as regression methods. Tests were performed selecting, for five distinct iterations, 80% of the available AS and healthy subjects to train the regressors, and the disjoint set with the remaining subjects for testing them. The obtained results are reported in terms of obtained root mean square error (RMSE) in Table IV, testifying that the considered signals have limited predictive capability regarding subjects' age, with a proportionate reduction of error (i.e., gain in predicting age when analyzing the collected signals) ranging from 2% to 47%, with better results achieved by jointly using both SCG and GCG data. The obtained results testify that, while the collected measurements allow to effectively distinguish between AS and healthy subjects, they may be scarcely correlated with their age, suggesting the relevance of the performed study on AS predictability also with the limits of the considered database.

On the other hand, results comparable with the performance we achieved were reported in similar studies that either required additional signals for classification (e.g., electrocardiogram or photoplethysmogram), or used SCG and GCG, even if collected through a single sensor placed at the center of the sternum (see Table V).

On the basis of our previous results demonstrating the possibility to accurately extract respiratory and cardiac information from GCG [28], [43], [44] without using ECG for segmenting the signal, further studies will be devoted to the use of additional features (e.g., respiratory rate, HR, linear and non-linear heart

rate variability indexes) in the classification algorithms to improve the overall classification performances. Additionally, in our research, we carried out a binary classification. Gathering data from a broader patient pool with varying degrees of AS, such as severe, moderate, and mild cases, would be beneficial for evaluating our proposed framework in a multi-class classification context. This would also aid in predicting specific hemodynamic parameters (like AVA) using SCG and GCG data.

V. CONCLUSION

The innovative approach of classifying AS patients using multi-site, multi-dimensional, ECG-independent measurements of cardiac-induced accelerations and angular velocities directly from the skin has shown promising results. By strategically placing just one or two sensors at the MV and PV levels, we can capture significant data. Our findings reveal that measurements taken from the X, AO, and TV levels offer limited insights compared to those from the MV and PV.

Interestingly, GCG data prove to be more insightful than SCG data. By combining these two types of signals and leveraging the unique strengths of both SVM and ResNet18 classifiers, our approach substantially boosts both the accuracy and reliability of patient classification. Recording data for just 40 s at the PV level, while simultaneously utilizing SCG and GCG data and combining the insights from both SVM and RN18 classifiers,

leads to a remarkable 97.2% accuracy in identifying patients with AS. This study is a step forward in the detection of AS and is essential for preventing irreversible disease progression and mortality because most patients with AS are asymptomatic.

CONFLICTS OF INTEREST

All authors declare no conflicts of interest.

AUTHOR CONTRIBUTIONS

The authors confirm their contribution to the paper as follows: Conceptualization, Carlo Massaroni, Gian Paolo Ussia, Annunziata Nusca and Emanuele Maiorana; methodology, Carlo Massaroni, Annunziata Nusca, Chiara Romano, Emiliano Schena, Sergio Silvestri and Emanuele Maiorana; Chiara Romano, Emanuele Maiorana and Carlo Massaroni; validation, Chiara Romano, Emanuele Maiorana and Carlo Massaroni; formal analysis, Chiara Romano, Emanuele Maiorana and Carlo Massaroni; investigation, Chiara Romano, Emanuele Maiorana and Carlo Massaroni; resources, Carlo Massaroni, Gian Paolo Ussia, Annunziata Nusca, Emiliano Schena, Sergio Silvestri; data curation, Chiara Romano, Simone Circhetta, Emanuele Maiorana and Carlo Massaroni; writing—original draft preparation, Chiara Romano, Simone Circhetta, Emanuele Maiorana, Annunziata Nusca and Carlo Massaroni; writing—review and editing, Gian Paolo Ussia, Emiliano Schena, Sergio Silvestri, Carlo Massaroni; visualization, Chiara Romano, Simone Circhetta, Emanuele Maiorana, Annunziata Nusca and Carlo Massaroni; supervision, Carlo Massaroni; project administration, Gian Paolo Ussia; funding acquisition, Carlo Massaroni, Emiliano Schena, Sergio Silvestri. All authors have read and agreed to the published version of the manuscript.

ACKNOWLEDGMENT

This work was supported in part by the European Project PROVIDE (“Prediction and prevention of cardiovascular diseases in pre- and type 2 diabetes”, call topic EU4H-2022-PJ-1) under Grant 101128983. Views and opinions expressed are however those of the author(s) only and do not necessarily reflect those of the European Union or the European Health and Digital Executive Agency (HADEA). Neither the European Union nor the granting authority can be held responsible for them.

REFERENCES

- [1] P. Carità et al., “Aortic stenosis: Insights on pathogenesis and clinical implications,” *J. Geriatr. Cardiol.*, vol. 13, no. 6, 2016, Art. no. 489.
- [2] S. Nathaniel, S. Saligram, and A. L. Innasimuthu, “Aortic stenosis: An update,” *World J. Cardiol.*, vol. 2, no. 6, 2010, Art. no. 489.
- [3] S. Stewart, C. Afoakwah, Y.-K. Chan, J. B. Strom, D. Playford, and G. A. Strange, “Counting the cost of premature mortality with progressively worse aortic stenosis in Australia: A clinical cohort study,” *Lancet Heal. Longevity*, vol. 3, no. 9, pp. e599–e606, 2022.
- [4] B. R. Lindman et al., “Calcific aortic stenosis,” *Nat. Rev. Dis. Primers*, vol. 2, no. 1, pp. 1–28, 2016.
- [5] N. M. Rajamannan, R. O. Bonow, and S. H. Rahimtoola, “Calcific aortic stenosis: An update,” *Nat. Clin. Pract. Cardiovasc. Med.*, vol. 4, no. 5, pp. 254–262, 2007.
- [6] V. Rizzello, “Moderate gradient severe aortic stenosis: Diagnosis, prognosis and therapy,” *Eur. Hear. J. Suppl.*, vol. 23, no. Supplement_E, pp. E133–E137, 2021.
- [7] R. A. Nishimura et al., “2017 AHA/ACC focused update of the 2014 AHA/ACC guideline for the management of patients with valvular heart disease: A report of the American college of cardiology/American heart association task force on clinical practice guidelines,” *Circulation*, vol. 135, no. 25, pp. e1159–e1195, 2017.
- [8] R. A. Nishimura et al., “2014 AHA/ACC guideline for the management of patients with valvular heart disease: A report of the American College of Cardiology/American Heart Association Task Force on Practice Guidelines,” *Circulation*, vol. 129, no. 23, pp. e521–e643, 2014.
- [9] M. J. Czarny and J. R. Resar, “Diagnosis and management of valvular aortic stenosis,” *Clin. Med. Insights Cardiol.*, vol. 8, 2014, Art. no. CMC-S15716.
- [10] J. Joseph, S. Y. Naqvi, J. Giri, and S. Goldberg, “Aortic stenosis: Pathophysiology, diagnosis, and therapy,” *Amer. J. Med.*, vol. 130, no. 3, pp. 253–263, 2017.
- [11] J. Minners, M. Allgeier, C. Gohlke-Baerwolf, R.-P. Kienzle, F.-J. Neumann, and N. Jander, “Inconsistencies of echocardiographic criteria for the grading of aortic valve stenosis,” *Eur. Heart J.*, vol. 29, no. 8, pp. 1043–1048, 2008.
- [12] P. Gjerdtsson, K. Caidahl, A. Odén, and O. Bech-Hanssen, “Diagnostic and referral delay in patients with aortic stenosis is common and negatively affects outcome,” *Scand. Cardiovasc. J.*, vol. 41, no. 1, pp. 12–18, 2007.
- [13] N. Saikrishnan, G. Kumar, F. J. Sawaya, S. Lerakis, and A. P. Yoganathan, “Accurate assessment of aortic stenosis: A review of diagnostic modalities and hemodynamics,” *Circulation*, vol. 129, no. 2, pp. 244–253, 2014.
- [14] E. J. Chun et al., “Aortic stenosis: Evaluation with multidetector CT angiography and MR imaging,” *Korean J. Radiol.*, vol. 9, no. 5, pp. 439–448, 2008.
- [15] J. Kwon et al., “Deep learning–based algorithm for detecting aortic stenosis using electrocardiography,” *J. Amer. Heart Assoc.*, vol. 9, no. 7, 2020, Art. no. e014717.
- [16] E. M. Johnson, A. J. Barker, J. D. Robinson, C. K. Rigsby, and M. Markl, “Elevated seismocardiography-derived chest energy is associated with aortic flow abnormalities in patients with aortic valve disease,” *Circulation*, vol. 146, no. Suppl_1, pp. A11504–A11504, 2022.
- [17] Z. Iftikhar et al., “Multiclass classifier based cardiovascular condition detection using smartphone mechanocardiography,” *Sci. Rep.*, vol. 8, no. 1, pp. 9344, 2018.
- [18] S. Mehrang et al., “Machine learning based classification of myocardial infarction conditions using smartphone-derived seismo-and gyrocardiography,” in *Proc. Comput. Cardiol. Conf.*, 2018, pp. 1–4.
- [19] T. Hurnanen et al., “Automated detection of atrial fibrillation based on time–frequency analysis of seismocardiograms,” *IEEE J. Biomed. Heal. Inform.*, vol. 21, no. 5, pp. 1233–1241, Sep. 2017.
- [20] M. J. Tadi et al., “Comprehensive analysis of cardiogenic vibrations for automated detection of atrial fibrillation using smartphone mechanocardiograms,” *IEEE Sens. J.*, vol. 19, no. 6, pp. 2230–2242, Mar. 2019.
- [21] T. Koivisto et al., “Mechanocardiography-based measurement system indicating changes in heart failure patients during hospital admission and discharge,” *Sensors*, vol. 22, no. 24, 2022, Art. no. 9781.
- [22] P. Reant et al., “Systolic time intervals as simple echocardiographic parameters of left ventricular systolic performance: Correlation with ejection fraction and longitudinal two-dimensional strain,” *Eur. J. Echocardiogr.*, vol. 11, no. 10, pp. 834–844, 2010.
- [23] A. Shokouhmand, N. D. Aranoff, E. Driggin, P. Green, and N. Tavassolian, “Efficient detection of aortic stenosis using morphological characteristics of cardiomechanical signals and heart rate variability parameters,” *Sci. Rep.*, vol. 11, no. 1, pp. 1–14, 2021.
- [24] C. Yang, B. Ojha, N. D. Aranoff, P. Green, and N. Tavassolian, “Classification of aortic stenosis before and after transcatheter aortic valve replacement using cardio-mechanical modalities,” in *Proc. IEEE 42nd Annu. Int. Conf. Eng. Med. Biol. Soc.*, 2020, pp. 2820–2823.
- [25] C. Yang, N. D. Aranoff, P. Green, and N. Tavassolian, “Classification of aortic stenosis using time–frequency features from chest cardio-mechanical signals,” *IEEE Trans. Biomed. Eng.*, vol. 67, no. 6, pp. 1672–1683, Jun. 2019.
- [26] M. J. Singh, S. Das, L. N. Sharma, and S. Dandapat, “Stationary wavelet transform based detection of aortic stenosis using seismocardiogram signal,” in *Proc. Nat. Conf. Commun.*, 2023, pp. 1–6.
- [27] C. Yang, B. D. Ojha, N. D. Aranoff, P. Green, and N. Tavassolian, “Classification of aortic stenosis using conventional machine learning and deep learning methods based on multi-dimensional cardio-mechanical signals,” *Sci. Rep.*, vol. 10, no. 1, 2020, Art. no. 17521.

- [28] C. Romano, D. Formica, E. Schena, and C. Massaroni, "Investigation of body locations for cardiac and Respiratory monitoring with skin-interfaced inertial measurement unit sensors," *IEEE Sensors J.*, vol. 23, no. 7, pp. 7806–7815, Apr. 2023.
- [29] D. M. Salerno and J. Zanetti, "Seismocardiography for monitoring changes in left ventricular function during ischemia," *Chest*, vol. 100, no. 4, pp. 991–993, 1991.
- [30] J. M. Zanetti and D. M. Salerno, "Seismocardiography: A technique for recording precordial acceleration," in *Proc. Comput.-Based Med. Syst.-Proc. 4th Annu. IEEE Symp.*, 1991, pp. 4–5.
- [31] R. S. Crow, P. Hannan, D. Jacobs, L. Hedquist, and D. M. Salerno, "Relationship between seismocardiogram and echocardiogram for events in the cardiac cycle," *Amer. J. noninvasive Cardiol.*, vol. 8, no. 1, pp. 39–46, 1994.
- [32] M. J. Tadi et al., "Gyrocardiography: A new non-invasive approach in the study of mechanical motions of the heart. Concept, method and initial observations," in *Proc. IEEE 38th Annu. Int. Conf. Eng. Med. Biol. Soc.*, 2016, pp. 2034–2037.
- [33] M. J. Tadi et al., "Gyrocardiography: A new non-invasive monitoring method for the assessment of cardiac mechanics and the estimation of hemodynamic variables," *Sci. Rep.*, vol. 7, no. 1, Dec. 2017, Art. no. 6823, doi: [10.1038/s41598-017-07248-y](https://doi.org/10.1038/s41598-017-07248-y).
- [34] P. Dehkordi, K. Tavakolian, M. J. Tadi, V. Zakeri, and F. Khosrow-Khavar, "Investigating the estimation of cardiac time intervals using gyrocardiography," *Physiol. Meas.*, vol. 41, no. 5, 2020, Art. no. 55004.
- [35] G. Santangelo, A. Rossi, F. Toriello, L. P. Badano, D. Messika Zeitoun, and P. Faggiano, "Diagnosis and management of aortic valve stenosis: The role of non-invasive imaging," *J. Clin. Med.*, vol. 10, no. 16, 2021, Art. no. 3745.
- [36] C. Massaroni, E. Cassetta, and S. Silvestri, "A novel method to compute breathing volumes via motion capture systems: Design and experimental trials," *J. Appl. Biomech.*, vol. 33, no. 5, pp. 361–365, 2017.
- [37] T. Hastie, R. Tibshirani, J. H. Friedman, and J. H. Friedman, *The Elements of Statistical Learning: Data Mining, Inference, and Prediction*, vol. 2. New York, NY, USA: Springer 2009.
- [38] O. Russakovsky et al., "ImageNet large scale visual recognition challenge," *Int. J. Comput. Vis.*, vol. 115, pp. 211–252, 2015.
- [39] K. He, X. Zhang, S. Ren, and J. Sun, "Deep residual learning for image recognition," in *Proc. IEEE Conf. Comput. Vis. Pattern Recognit.*, 2016, pp. 770–778.
- [40] C. Szegedy, V. Vanhoucke, S. Ioffe, J. Shlens, and Z. Wojna, "Rethinking the inception architecture for computer vision," in *Proc. IEEE Conf. Comput. Vis. Pattern Recognit.*, 2016, pp. 2818–2826.
- [41] G. Huang, Z. Liu, L. Van Der Maaten, and K. Q. Weinberger, "Densely connected convolutional networks," in *Proc. IEEE Conf. Comput. Vis. Pattern Recognit.*, 2017, pp. 2261–2269.
- [42] I. Elnaggar et al., "Detecting aortic stenosis using seismocardiography and gyrocardiography combined with convolutional neural networks," *Comput. Cardiol.*, pp. 1–4, 2021.
- [43] Č. Milena et al., "Linear and non-Linear heart rate variability indexes from heart-induced mechanical signals recorded with a skin-interfaced IMU," *Sensors*, vol. 23, no. 3, 2023, Art. no. 1615.
- [44] C. Romano, E. Schena, D. Formica, and C. Massaroni, "Comparison between chest-worn accelerometer and gyroscope performance for heart rate and respiratory rate monitoring," *Biosensors*, vol. 12, no. 10, 2022, Art. no. 834, doi: [10.3390/bios12100834](https://doi.org/10.3390/bios12100834).

Open Access funding provided by 'Università "Campus Bio-Medico" di Roma' within the CRUI CARE Agreement